Machine Vision and Applications (2011) 22:927–945
DOI 10.1007/s00138-010-0287-7

ORIGINAL PAPER

Road environment modeling using robust perspective analysis and recursive Bayesian segmentation

Marcos Nieto · Jon Arróspide Laborda · Luis Salgado

Received: 21 July 2009 / Revised: 8 April 2010 / Accepted: 5 July 2010 / Published online: 8 August 2010

Abstract Recently, vision-based advanced driver-assistance systems (ADAS) have received a new increased interest to enhance driving safety. In particular, due to its high performance–cost ratio, mono-camera systems are arising as the main focus of this field of work. In this paper we present a novel on-board road modeling and vehicle detection system, which is a part of the result of the European I-WAY project. The system relies on a robust estimation of the perspective of the scene, which adapts to the dynamics of the vehicle and generates a stabilized rectified image of the road plane. This rectified plane is used by a recursive Bayesian classifier, which classifies pixels as belonging to different classes corresponding to the elements of interest of the scenario. This stage works as an intermediate layer that isolates subsequent modules since it absorbs the inherent variability of the scene. The system has been tested on-road, in different scenarios, including varied illumination and adverse weather conditions, and the results have been proved to be remarkable even for such complex scenarios.

Keywords ADAS · Real-time · Plane rectification · Bayesian segmentation · Kalman filtering · Multi-domain vehicle tracking

1 Introduction

On-board advanced driver-assistance systems (ADAS) have been receiving increasing attention from the intelligent transportation system (ITS) community (car manufacturers, research centers and users) due to their ability to provide useful information about the vehicle environment by functioning as sensors for services such as lane departure warning, collision avoidance, stop-and-go, etc. In particular, the solutions based on video processing have played an important role in this field since the past decade, due to their low cost, the increased performance of microprocessor systems, and the research advances in the field of computer vision [1].

The on-board scenario poses a number of challenges for vision systems, as it is an extremely varied environment [2]. For instance, it involves sudden and significant illumination changes (as when entering into tunnels), different types of road pavement, or the appearance of lane markings, which may have contrasts that vary significantly from one road to another. Moreover, weather conditions may also affect vision systems. For example, the image could contain rain drops, moving wipers, etc. Additionally, the motion of the scene entails more complexity, as it is composed of the motion induced by the vehicle itself with respect to static elements, and of other vehicles, typically moving at different speeds.

The most recent trends in this field have focused on 3D environment modeling using stereovision systems, due to their ability to recover depth information from the analysis of two synchronized video inputs. For instance, several works address sub-pixel accuracy lane markings models [3–5] using calibration information. Others use image alignment between the stereo pair to detect volumetric objects on the road plane [6,7], or to enhance lane marking detection [8].

While showing promise in obtaining depth information, stereoscopic vision has a number of drawbacks: multi-view systems are typically not considered for real-time applications due to their built-in complexity, which is mainly related to the calibration process, the necessity of a synchronized acquisition system, and the difficulties encountered in finding reliable correspondences between images [9]. Mono-camera

M. Nieto (✉) · J. Arróspide Laborda · L. Salgado
Grupo de Tratamiento de Imágenes,
Universidad Politécnica de Madrid, Ciudad Universitaria s/n,
ETSIT C-306, 28040 Madrid, Spain
e-mail: mnd@gti.ssr.upm.es

systems are more cost-effective and hence more widely used in real applications [10]. Different mono-camera approaches have been proposed in the literature to address the road modeling [11], including accurate lane markings models [12,13], and vehicle detection and tracking [14–17].

Some of these solutions provide coarse or incomplete results due to the intrinsic limitations of the mono-camera analysis: projective geometry is typically handled using appearance-based methods that may be faster than stereo [18] without evaluating the loss in robustness. However, some researchers compensate for this limitation by making prior assumptions about the environment, for example, by defining a constant relative pose of the camera with respect to the road [11,19]. However, such approaches reduce the system's capability to adapt to more realistic situations.

In this paper we propose a new mono-camera system, which is the result of the research work carried out during the European I-WAY project. It provides an accurate and very complete environment model that dynamically adapts to changes in the scenario and that minimizes the use of prior information. This approach comprises robust strategies that ensure reliable real-time operation in real driving situations.

Our approach is fully adaptive to the unknown scenario conditions, without using prior information about the pose of the camera with respect to the road, which as opposed to most approaches in the literature is automatically retrieved through an adaptive computation of the image-plane to road-plane homography [2,20]. This transform, which is stabilized using a dynamic vanishing point estimation method, removes the inherent perspective distortion from the images and thus simplifies further analysis stages.

The adaptability to the extremely variable on-road environment is given by a MAP probabilistic framework, which is the major contribution of this paper, since it allows to integrate models of different elements of the road altogether in a simple way, allowing to overcome the need to handle multiple detectors for each targeted element (vehicles, lane markings, pavement, etc.). This framework operates on the transformed domain and segments the elements of the road according to a set of dynamic likelihood and prediction models that are updated through the observation of different features extracted from the images. This stage can be seen as a layer that absorbs the dynamism of the input images, including illumination changes, rapid motion objects, or sudden changes of the appearance of the road. The output are steady segmented images that facilitate the subsequent modeling tasks, which do not have to care about the complexity of the observations.

The description of the road environment delivered by the modeling stages takes into consideration a wide variety of useful information for ADAS. This information is related to both static and dynamic elements of the environment, e.g., the lanes and their geometry, and mainly, the vehicles on the road. These elements are described using appearance-based models that are dynamically updated through stochastic filtering, which enhances the accuracy and completeness of the results. Most remarkably, a cooperative analysis of the original and transformed domain is exploited to overcome the intrinsic limitations of each domain.

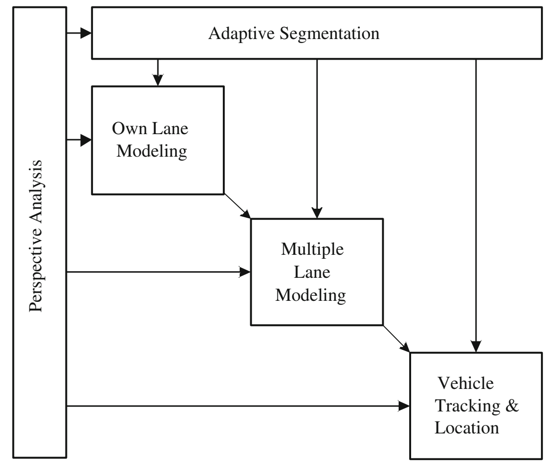

Fig. 1 Block diagram of the proposed Road Modeling system

The system has been tested on-road, and has proved to perform in real-time and to provide accurate and reliable results for a set of different environments, including variable illumination and adverse weather conditions, heavy traffic, different types of roads, different pavement colors, etc.

2 System overview

The system aims to provide a full description of the scenario ahead of the vehicle, i.e., a model of the road and the vehicles in it, in real-time. The block diagram of the system is shown in Fig. 1. The processing is divided into three core blocks: perspective analysis, recursive Bayesian segmentation, and scene modeling. For each incoming image, the geometry of the scene is analyzed in order to derive a transformation that removes perspective distortion from the image. As a result, a fronto-parallel view of the road ahead is obtained in which road elements (i.e., lane markings) and vehicle dynamics are proportional to their real appearance and behavior, as shown in Fig. 2. Then, the image in the transformed domain is segmented through a Bayesian classifier that uses a parametric multiple-class likelihood model of the road. The pixels in the image are thus classified as belonging to pavement, lane markings, dark objects or to unknown elements not classifiable as any of the previous (see Fig. 2c).

In the final stage, a full description of the scene elements is provided, using the information obtained in the segmentation image and the defined models. This stage consists of two parallel analysis modules: road modeling and vehicle detection

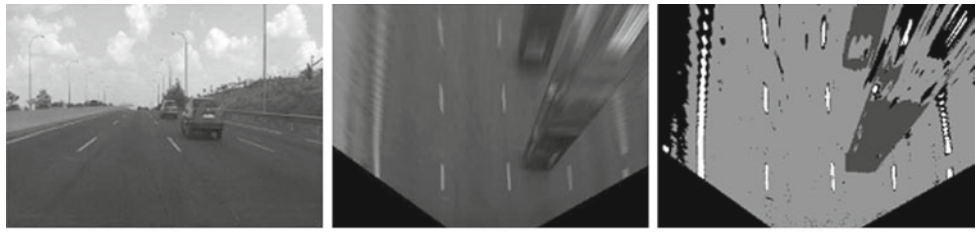

Fig. 2 Segmentation process: **a** original image; **b** road-plane; and **c** four-level segmentation (in *black* for unknown elements)

and tracking. In the former, novel lane tracking and model fitting techniques allow to obtain precise information of the own and adjacent lanes. In turn, vehicle detection and tracking strategy relies on a collaborative approach between the original and the transformed domains. Additionally, a feedback loop allows to use vehicle detection results as an input for segmentation of the following images, thus exploiting their underlying temporal coherence. Eventually, the output of both modules is combined to produce high level information, such as detections of lane changes of the own or other vehicles, vehicle trajectories, etc.

3 Perspective analysis

An important perspective distortion arises in images captured from cameras moving in the direction of the optical axis, as shown in the example in Fig. 2a. There are a number of benefits derived from the removal of this effect in road scenarios, available through the computation of a virtual fronto-parallel view of the road ahead (typically denoted as "bird's-eye view" or "Inverse Perspective Mapping") [2,21]: lane markings are parallel in this domain, lanes are imaged with their actual width (up to scale), the complexity of the curve analysis is reduced and also the relative speed and position of the vehicles are imaged without distortion, with magnitudes proportional to the actual ones on the road.

Many works, especially the former on plane rectification [2], assumed the prior knowledge of all the parameters of the projective matrix: i.e., the camera calibration matrix as well as the relative rotation and translation of the camera with respect to the road plane.

These type of assumptions might be valid for surveillance systems that do not model the dynamism of the road scenario, but in on-board systems it can lead to large errors in the rectification, due to the steering of the vehicle, its bumping, or slope changes. Some authors have studied the dependence of the obtained transform image according to the variability of the environment. For instance, [31] analyzes the impact of the pitch and yaw angles in the obtained rectified image in terms of radial distortion and parallelism. In this line, different authors have identified the pitch angle error (i.e. the error between the instantaneous pitch angle and that used to perform rectification), as the main cause of the image distortion, and have proposed methods to minimize this error. Jiang [18] computes the rectification with fixed parameters and checks the parallelism between the left and right lane markings, estimated as straight lines, corrects the angles, and re-estimates the rectification. Cerri [30] computes several rectifications using a range of pitch values, and then also checks the parallelism between the detected lane markings to determine which pitch angle was the correct one.

In this work, we propose to update the values of both the pitch and yaw angles at each time instant by means of the robust computation of the dominant vanishing point of the scene, given by the intersection of the lane markings. Hence, in contrast to most approaches our method represents a flexible and robust alternative to perform plane rectification.

3.1 Pinhole camera projection

The projection process that generates the image shown in Fig. 2b is described as a linear process using homogeneous coordinates for both the points in the 3D space and the image coordinates [22]. If we define a point in the 3D world as $\mathbf{X}$ in homogeneous coordinates, its projection into the image plane combines two transforms: the former converts the point into the camera coordinate system, yielding $\mathbf{X}_c$, and the second projects it into the image plane, $\mathbf{x}$. The combination of these steps renders the following expression:

$$\mathbf{x} = \mathrm{K}\mathbf{X}_c = \mathrm{K}(\mathrm{R}| - \mathrm{R}\mathbf{c})\mathbf{X} = \mathrm{P}\mathbf{X} \tag{1}$$

where P is the so-called projection matrix, K is the camera calibration matrix, and R and $\mathbf{c}$ are the aforementioned relative rotation and translation, respectively, between the world and camera coordinate systems. These concepts are illustrated in Fig. 3.

If we now consider points in the 3D space that correspond to the road plane (i.e., with spatial coordinate $Y = 0$), and define $\mathbf{p}_i$ as the i-th column of P we arrive at the following expression:

$$\mathbf{x} = \mathrm{P}\begin{pmatrix} X \\ 0 \\ Z \\ 1 \end{pmatrix} = (\,\mathbf{p}_1\ \mathbf{p}_3\ \mathbf{p}_4\,)\begin{pmatrix} X \\ Z \\ 1 \end{pmatrix} = \mathrm{H}\mathbf{x}' \tag{2}$$

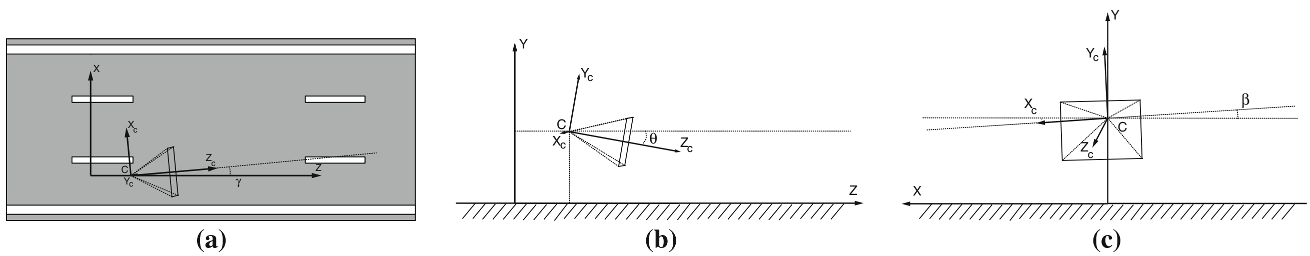

Fig. 3 Yaw (γ), pitch (θ) and roll (β) angles, respectively in **a**, **b**, and **c** within the defined road scenario. The camera coordinate system is shown as $\{X_c, Y_c, Z_c\}$

which yields the target plane to plane homography H between the coordinates of the points of the road plane, $\mathbf{x}'$, and the points on the image plane, $\mathbf{x}$.

Therefore, we can compute the homography that leads to the rectified domain by computing the unknown parameters of the projection matrix P, which are, in our case, the rotation angles. The rest of parameters can be considered fixed and known, like the camera calibration matrix K, which is computed off-line, and the translation $\mathbf{c}$, as the camera moves rigidly with respect to the vehicle.

Since the camera is installed inside the vehicle with null roll angle, the problem is significantly simplified. This assumption holds if the camera is carefully installed without rotation with respect the Z-axis, and implies that the horizon line is actually horizontal. Hence, if we determine the position of the horizon in the image (by estimating its coordinate in the Y-axis), we have recovered the affine properties of the plane, e.g., parallelism, area ratios, as well as the angular information, provided that we know the camera calibration matrix.

This way it is enough to compute the vanishing point associated with the lane markings of the road, that we will call $\mathbf{v}_z = (v_{z,1}, v_{z,2}, 1)^\top$, which belongs to the line at the infinity and thus defines it completely. The computation of the vanishing point is addressed in the following section.

The vanishing point is then projected into the camera coordinate system as $\mathbf{v}'_z = \mathrm{K}^{-1}\mathbf{v}_z$, so that the pitch and yaw angles can be directly computed as

$$\theta = \arctan(v'_{z,2}); \quad \gamma = \arctan\left(-\frac{v'_{z,1}}{\cos\theta}\right) \tag{3}$$

These expressions come from the following argument: consider the point at the infinity corresponding to the vanishing point $\mathbf{v}_z$, and its projection into the image plane as

$$\mathbf{v}_z = \mathrm{K}(\mathrm{R}|-\mathrm{R}\mathbf{c})\begin{pmatrix}0\\0\\1\\0\end{pmatrix} = \mathrm{K}\begin{pmatrix}\tan\gamma\cos\theta\\ \tan\theta\\ 1\end{pmatrix} \tag{4}$$

so that if we consider that we know the camera calibration matrix and we left-multiply both sides of (4) by K^{-1} we obtain $\mathbf{v}'_z = (\tan\gamma\cos\theta, \tan\theta, 1)^\top$, which are two equations on the two unknowns θ and γ, solved using the Eq. (3).

Figures 4 and 5 show two example sequences representing two typical situations. The former depicts a lane change manoeuver, where the vehicle is steering at the right and makes two consecutive lane changes. As shown in Fig. 4, the height of the vanishing point, $v_{z,2}$ is almost constant, apart from some detection noise, and so is the pitch angle. The transversal position of the vanishing point, $v_{z,1}$, changes, indicating a significant change of the yaw angle. This is maximum when the vehicle is at maximum steer, and returns to its initial values as the vehicle stabilizes its position within a lane.

The second example, shown in Fig. 5 illustrates the behavior of the vanishing point in a significant road slope. The pitch angle is the one that varies more significantly, following the movement of the vertical component of the vanishing point, $v_{z,2}$. The yaw angle is steady, since although it depends on the variation of the pitch angle, its influence is highly attenuated by the arctangent expression shown in Eq. (3).

As a result, we obtain rectified images of planes which show parallel lane markings, with constant width, even in difficult situations where the described extrinsic parameters vary.

3.2 Vanishing point estimation

As stated in the previous section, the correct estimation of the vanishing point along time is a key step towards the adaptability and stability of the system. For this purpose, we have designed a robust method for vanishing point estimation. It is based on a specific lane marking detector that provides instantaneous measurements about the vanishing point, and on a Kalman filter that provides temporal coherence to the measurements, and also allows to control the putative outliers.

Lane markings can be approximated as straight lines in the lower part of the image, even in the presence of significant curvature ahead. The detection is done using a specific lane marking detector, which is applied to each row of the image, assuming that the appearance of the lane markings in this

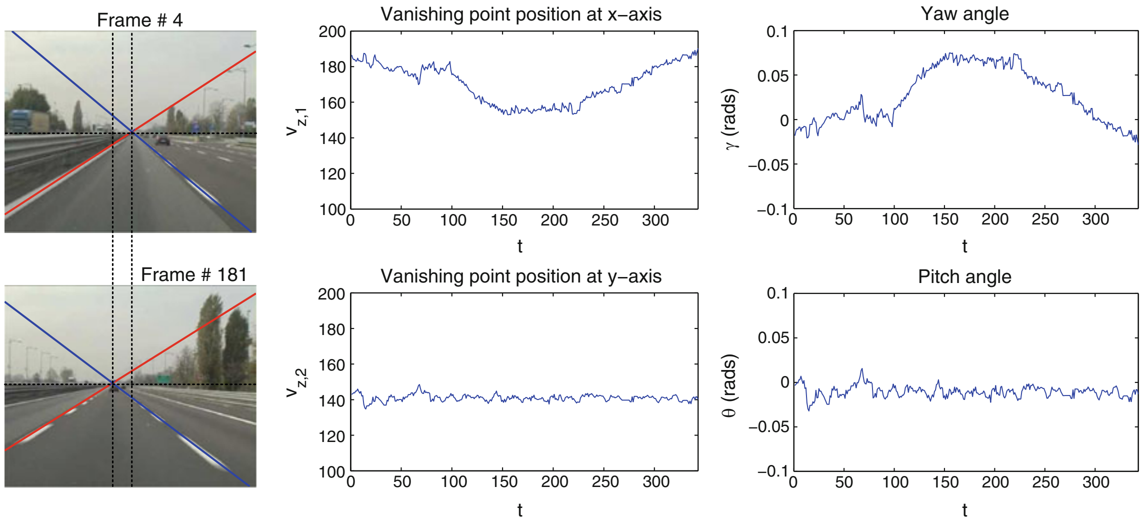

Fig. 4 Example of variation of the pitch and yaw angle in a lane change manoeuver. The vanishing point is shown as the intersection of *two colored lines* for a better visualization (color in online)

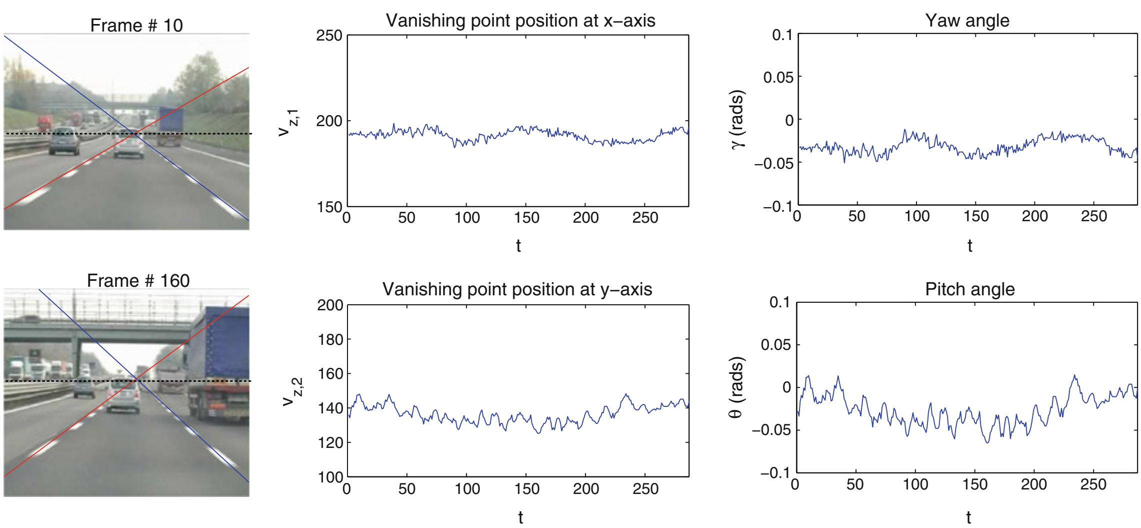

Fig. 5 Example of variation of the pitch and yaw angle in a road slope change

one-dimensional domain is given by pulses of high intensity values surrounded by darker regions. Therefore, the analysis is done by independently filtering each image row of intensity values, denoted as $\{x_i\}_{i=1}^{W}$, resulting in a new filtered data array $\{y_i\}_{i=1}^{W}$, defined as

$$y_i = 2x_i - (x_{i-\tau} + x_{i+\tau}) - |x_{i-\tau} - x_{i+\tau}| \tag{5}$$

where τ is the width parameter that governs the filtering process. This filter produces high responses for positions with x_i values that are higher than those of their neighbors on the left and right at a distance τ. The last term in (5) penalizes cases in which the difference between the left and right neighbors is high, so that a higher response is given to positions with similar left and right neighbors. This last term makes this filter less prone to errors than other lane marking detectors presented in the literature [2,20]. An example is given in Fig. 6: the original and filtered images of a typical road scene are shown, and two different rows are analyzed, showing both the intensity of the original image and the result of the filter in each row. Row 2 exemplifies the excellent performance of the detector, even with obstructing elements, such as the wiper of the vehicle. The scenario of Row 1 is more challenging, as there are several abrupt changes in the intensity profile, due to the presence of vehicles. Nevertheless, as shown in the response profile, our method accurately detects the lane marking of interest and dismisses the superfluous information.

The well known Hough transform [23] is then used to detect lines in the resulting image. This transform is robust against outliers and provides multiple line fitting. Each line

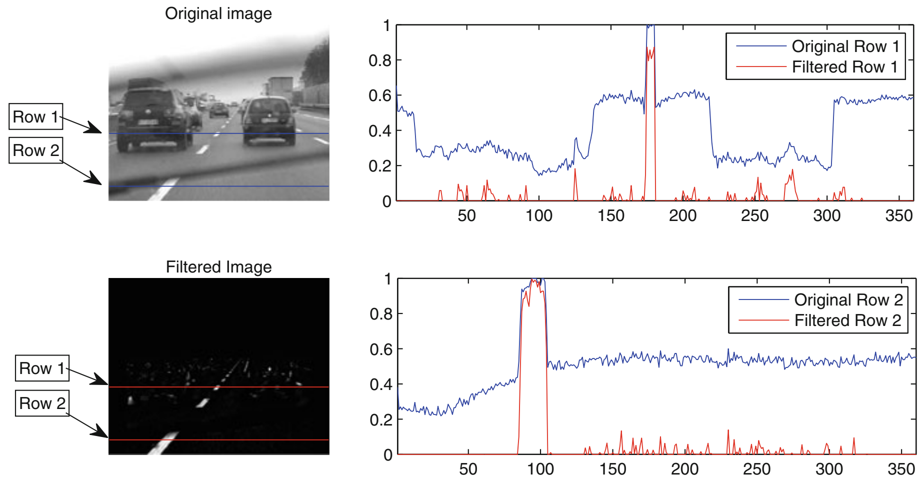

Fig. 6 Lane marking detector example. For clarity, the response to the filter has been normalized between 0 and 1

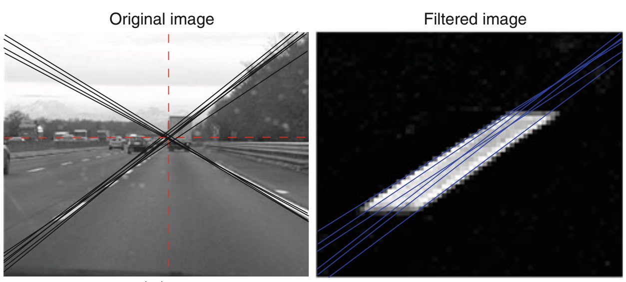

(a) **(b)**

Fig. 7 Hough transform applied to the image result of the lane marking detector: **a** least squares vanishing point depicted as the intersection of the *red lines*; and **b** a zoom of a lane marking for which several lines have been fitted (color in online)

is parameterized with an angle θ and a distance ρ as $x \sin\theta + y \cos\theta = \rho$.

The Hough transform may give more than two lines for each lane marking, which result in multiple intersection points, as shown in Fig. 7. We apply here a robust scheme that allows us to filter the lines delivered by the Hough transform, in order to remove the putative outliers that would significantly affect the least squares solution. The RANSAC algorithm is used to classify lines into inliers and outliers. This algorithm works iteratively, by selecting, at each iteration, a pair of lines and computing its intersection point. The lines whose distance to this point are less than a given error threshold are computed as inliers, and denoted as the consensus set of the hypothesis. RANSAC iterates until the probability of finding a better consensus set is below some convergence threshold (typically 5%).

This way, the outliers are removed from the set of lines, and we can compute the vanishing point $\mathbf{v}_z$, without risks, as the solution of the system of equations built with the equations of each detected line:

$$\left[\,\mathbf{s} \mid \mathbf{c}\,\right]\mathbf{v} = \mathbf{p} \tag{6}$$

where $\mathbf{s} = (\sin\theta_0, \ldots, \sin\theta_{l-1})^\top$, $\mathbf{c} = (\cos\theta_0, \ldots, \cos\theta_{l-1})^\top$, $\mathbf{p} = (\rho_0, \ldots, \rho_{l-1})^\top$, and l is the number of lines. The least squares solution is obtained with SVD. Figure 7 shows an example of the computation of the vanishing point for a typical road scene.

Each instantaneous estimate of the vanishing point obtained, as described earlier, is treated as a noisy measurement, which is then introduced into a Kalman filter to provide a better estimation of the vanishing point.

Briefly, this approach stabilizes the coordinates of the detected vanishing point by adding temporal coherence to the estimation process. The dynamic model used is a constant-velocity model, with the state vector $\mathbf{s}_k = (v_x, v_y, \dot{v}_x, \dot{v}_y)^\top$. This model is explained in more detail in Sect. 5.1.

4 Recursive Bayesian segmentation

The segmentation algorithm used in this work is based on the Bayesian decision theory. The algorithm defines a parametric multiple-class likelihood model of the road, from which pixels are classified into different classes, with an associated probability of error.

Three types of elements of interest are considered within any road-plane image:

- **Pavement**: light gray regions of the road.
- **Lane markings**: bright stripes painted on the road.
- **Objects**: dark elements, such as the lower parts of vehicles, their wheels, shadows, etc.

The probabilistic framework handles all the available information in a simple and robust way, by defining the prior probabilities and the likelihood models, and by appropriately choosing the features that best characterize the classes that are to be identified. Therefore, it avoids defining and computing a large amount of deterministic cases or situations

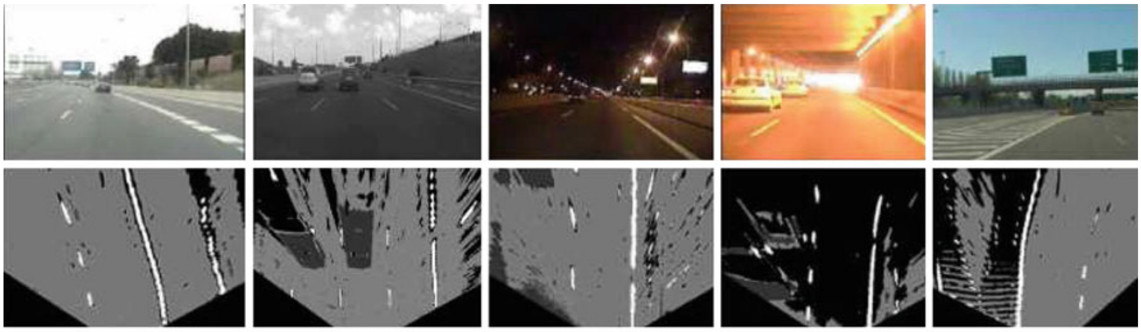

Fig. 8 Example of the application of the Bayesian classifier to the transformed domain: *upper row* contains images corresponding to very different scenarios; and *lower* contains the segmented images. Note that the result is very accurate for all of them, except for the tunnel sequence, in which the sudden illumination changes makes the classifier to set to unknown most of pavement pixels. Nevertheless, this does not affect either the lane markings or the vehicle detection stages

regarding illumination conditions, presence of vehicles, motion, etc.

Besides, classical approaches tend to classify pixels as strictly belonging to one of the aforementioned elements. In contrast, we make use of an additional "unknown" class, which gathers the pixels which do not match the models defined for the sought elements. This is quite frequent in outdoor uncontrolled environments, where additional elements such as median stripes or guard rails can appear. The proposed method considers these cases and hence avoids classification error.

4.1 Bayesian framework

Let $\mathcal{S} = \{P, L, O, U\}$ be the set of classes that represent, respectively, the pavement, lane markings, objects, and the unidentified elements. The target of the classifier is to assign one of these classes to each pixel of the image.

Let X_i represent the event that a pixel, indexed with its spatial coordinates inside the image (x, y), with an associated observation vector denoted as $\mathbf{z}_{xy}$, is classified as belonging to the class $i \in \mathcal{S}$. Using the Bayesian decision theory, this classification is carried out by selecting the class that maximizes the a posteriori conditional probability $P(X_i|\mathbf{z}_{xy})$, which is decomposed by the Bayes' rule as

$$P(X_i|\mathbf{z}_{xy}) = \frac{p(\mathbf{z}_{xy}|X_i)P(X_i)}{P(\mathbf{z}_{xy})} \tag{7}$$

where $p(\mathbf{z}_{xy}|X_i)$ is the likelihood function, i.e., the probability that a pixel, according to its associated measurements, belongs to class i; $P(X_i)$ is the prior probability of each class and $P(\mathbf{z}_{xy})$ is the evidence, computed as $P(\mathbf{z}_{xy}) = \sum_{i \in \mathcal{S}} p(\mathbf{z}_{xy}|X_i)P(X_i)$, which is a scale factor that ensures that the posteriors sum to unity.

The result, for each pixel, is a set of posterior probabilities $\{P(X_i|\mathbf{z}_{xy})\}_{i \in \mathcal{S}}$, which denote the probability that a pixel belongs to each defined class. Accordingly, each pixel of the image is classified as the class with the maximum posterior probability. The likelihood and the prior probabilities are computed as described in the following subsections.

Figure 8 shows the resulting four-level segmentation for a number of example images. As shown, the segmentation is applied to the road plane image after the perspective transform is computed. In the segmented image, for clarity, the pixels have been colored according to their classification: the white pixels belong to the lane markings, the light gray pixels are those that likely belong to the pavement of the road, and the dark gray pixels are those that are assigned to the wheels and shadows of the lower parts of the vehicles. The black pixels are those that have not been classified as belonging to any of the three previous classes, and therefore remain as unknown pixels.

4.2 Likelihood models

In this section the likelihood models are described as parametric functions, according to the expected properties of the considered image features with respect to the defined classes. Additionally, the estimation of their parameters is obtained through an optimization process using the Expectation-Maximization (EM) algorithm.

The basic appearance of the defined classes may be described as follows: the pavement is usually a homogeneous area in the transformed image, sharing a common intensity level with low variations among pixels; the lane markings are represented as near-vertical bright stripes, usually surrounded by pavement pixels; and objects typically can be characterized by dark regions with intensity levels lower than the pavement (note that even white vehicles contain dark areas in their lower part due to shadows and wheels).

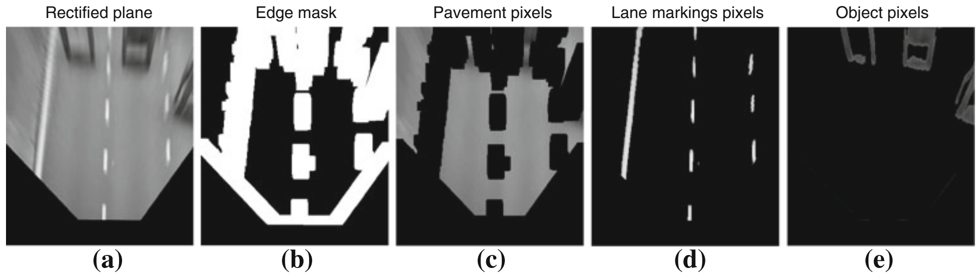

Fig. 9 Initialization of the parameters of the likelihood function for the intensity feature

With this information, it is possible to design pixel-level features that help to differentiate between classes. Two features have been used for this purpose: the intensity or grayscale level, I_{xy}, and the response to the lane marking detector, L_{xy}. The combination of these features ensures a clear class differentiation, especially accurate for the lane markings class, thus allowing to reduce misclassifications. The likelihood function of class i is defined as the product of the likelihood functions for each image feature assumed to be conditionally independent: $p(\mathbf{z}_{xy}|X_i) = p(I_{xy}|X_i)\, p(L_{xy}|X_i)$.

4.2.1 Intensity feature

The likelihood functions for I_{xy} are all defined as normal distributions. In particular, the likelihood of the pavement class is

$$p(I_{xy}|X_P) \propto \exp\left(-\frac{1}{2\sigma_{I,P}^2}(I_{xy} - \mu_{I,P})^2\right) \tag{8}$$

where $\mu_{I,P}$ and $\sigma_{I,P}$ are the mean and standard deviation of the distribution. The likelihood distributions of the other classes are parameterized analogously as $\{\mu_{I,L}, \sigma_{I,L}\}$, $\{\mu_{I,O}, \sigma_{I,O}\}$ and $\{\mu_{I,U}, \sigma_{I,U}\}$. Note that there is an implicit necessary condition that must be satisfied: $\mu_{I,O} < \mu_{I,P} < \mu_{I,L}$, since the dark objects are always darker, as well as lane markings are always clearer than the pavement. The model for the unknown class is defined as a normal distribution with large fixed variance, so that it is similar to a uniform distribution.

4.2.2 Lane marking detector

Regarding the likelihood functions associated with the proposed detector, lane markings are expected to provide high response values to the filter and low response values for the other classes. This way, the likelihood functions for L_{xy} are defined as normal distributions. The parameters of the distributions are $\{\mu_{L,P}, \sigma_{L,P}\}$, $\{\mu_{L,L}, \sigma_{L,L}\}$, $\{\mu_{L,O}, \sigma_{L,O}\}$ and $\{\mu_{L,U}, \sigma_{L,U}\}$. The unknown class must be modeled with wide normal distribution, in the same manner as explained for the intensity feature.

For this feature, the conditions are $\mu_{L,O} < \mu_{L,L}$ and $\mu_{L,P} < \mu_{L,L}$, which mean that lane markings have always higher values for this feature than pavement and dark objects.

4.2.3 Parameters estimation

The parameters of the aforementioned functions are computed for each image of the sequence. Hence, the system dynamically adapts the Bayesian model in a sequential manner.

The EM algorithm for a mixture of Gaussians is used to estimate the parameters that govern the likelihood functions for the defined classes since we defined all of them as normal distributions. The EM algorithm converges to the optimal solution if it is given a good initialization or start point. In effect we can provide coarse estimates for these parameters through the application of a preliminary analysis of the histogram of the image (an example image is given in Fig. 9a and its associated histogram is shown in Fig. 10a). The approach extracts three groups of pixels from the image, one for each class. First, the putative pixels of the pavement class are obtained by dismissing pixels with high gradient. For that purpose a mask is generated as shown in Fig. 9b, which is used to remove the pixels with high gradient and their neighborhood[1]. The value of the parameters for $p(I_{xy}|X_P)$ are then obtained as the sample mean and the sample standard deviation of the pixels of the resulting group, shown in Fig. 9c.

The lane marking and object classes are then extracted by thresholding the road-plane image at $\mu_{I,P} \pm 3\sigma_{I,P}$, respectively. These thresholds were chosen to satisfy the hypotheses $\mu_{I,O} < \mu_{I,P} < \mu_{I,L}$. In particular, the selection of $\mu_{I,P} \pm 3\sigma_{I,P}$ dictates that only those pixels falling outside the 99, 999% of the probability of belonging to the pavement are considered for modeling the two other classes.

The images in Fig. 9d, e show the corresponding sets of pixels that likely belong to the lane markings, and the objects class for an example image. The corresponding histograms for the images in Fig. 9 c–e are shown in Fig. 10b–d,

[1] We have done this by applying first a Sobel gradient detection, an appropriate thresholding and a morphological dilation.

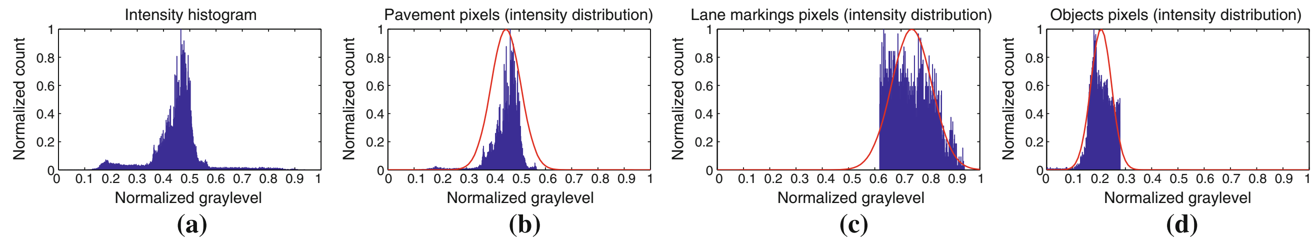

Fig. 10 Histograms of the different sets of pixels for the computation of the likelihood parameters for I_{xy}

respectively, with the associated normal fit that depicts the mean and standard deviation value that describe the histograms.

Regarding the lane marking detector feature, a similar approach is followed. The images L_{xy} are first computed, and their histograms are assumed to be a mixture of two Gaussians, one of them centered near zero (corresponding to the low response of pavement and object pixels to the lane marking filter), and the other, with much larger variance, covering the tail of the histogram (which implies that lane markings obtain high response to the filter, although ranging from moderate to very high values). A reasonable threshold that separates these two components is the standard deviation of the distribution. Once the images are separated, the mean and standard deviation for the corresponding sets of pixels can be computed, obtaining $\{\mu_{L,L}, \sigma_{L,L}, \mu_{L,P} = \mu_{L,O}, \sigma_{L,P} = \sigma_{L,O}\}$. Note that for this feature, the pavement and objects class cannot be distinguished and hence sharing the parameters of the likelihood function.

Within the EM algorithm, the likelihood functions according to the two defined features (intensity and response to the lane markings detector) are modeled as a mixture model:

$$p(I_{xy}|\{X_i\}_{i\in\mathcal{S}}) = \sum_{i\in\mathcal{S}} \omega_{i,L}\, p(I_{xy}|X_i) \tag{9}$$

$$p(L_{xy}|\{X_i\}_{i\in\mathcal{S}}) = \sum_{i\in\mathcal{S}} \omega_{i,I}\, p(L_{xy}|X_i) \tag{10}$$

where $\omega_{i,I}$ and $\omega_{i,L}$ are the weights of the corresponding mixture components. These coefficients represent the proportion of elements of the set (in this case the pixels of the image) that belong to each class. In our approach, the EM algorithm considers as initialization for these coefficients the actual proportion obtained in the classification of the previous time instant and estimates the new values for the current instant.

The EM algorithm iterates until the whole set of parameters, including the mean and standard deviation of each normal distribution and the mixture component weights are computed. The E-step and M-step for a mixture of Gaussians are well-known problems in many computer vision applications. Their expressions can be found in [24]. As an exception, the unknown class is kept fixed, and not updated within the EM framework to ensure that a quasi-uniform distribution absorbs the putative outliers.

Finally, the system comprises a control mechanism that is able to detect situations involving sudden visibility or illumination changes, such as when entering or exiting tunnels. In these situations, the system switches to a transitory state, in which the variables are not updated according to observations in order to prevent the system from being corrupted. Meanwhile the images are checked, and the transitory state finishes when the situation is stabilized. This control scheme hence increases the overall robustness of the system, and avoids misleading the EM algorithm with wrong initializations.

4.3 Prior probabilities

The prior probability of each defined class must be computed in order to obtain the final posterior probability for each pixel of the image. These prior probabilities represent prior knowledge of the probability of a pixel to belong to each class before examining its associated observations. Typically, prior information is obtained from the posterior probabilities from previous time instants, through the so-called dynamic or prediction models.

Different source information can be used to generate prior models. Specifically, if an estimation of the ego-motion of the camera is available[2], we can generate prior probability maps from the previous time instant posterior probabilities applying a translation that compensates the ego-motion and adding some Gaussian blurring.

In the case in which there are vehicles in the scene, we use their prediction model, as we shall explain in Sect. 6, which defines the regions of the image that are more likely to contain vehicles in the next image via a binary mask. The prior information of each pixel for each class can be multiplied by the value of the corresponding pixels of the mask. Hence, the probability to belong to one of these classes of the pixels that belong to the black region of the mask (as shown in Fig. 11b), is set to a low value (typically 0.1, such that the prior for class vehicle is 0.9 for these pixels). As a result, the pixels of this

[2] It can be obtained easily from the rectified images through the computation of a simple translation plus rotation motion model, for instance, with point correspondences between consecutive images.

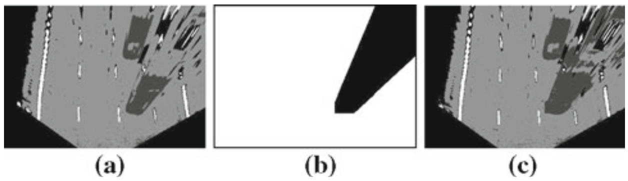

Fig. 11 Prior probability map provided by vehicle tracking

black region will be more easily classified as belonging to the object class by the prior maps. Figure 11 shows in c and a, respectively, the segmentation results obtained with and without the use of this prediction model.

5 Road-plane element modeling

The information regarding lane markings and pavement given by the segmentation is used to estimate the presence and geometry of the lanes of the road. Our approach successfully deals with challenging elements, such as curvature, an unknown number of lanes, lane changes, poorly painted lane markings, and lanes of variable width, as well as emerging and splitting lanes. The following sections describe the "lane tracker" technique that we use to detect and track the position of the ego-vehicle inside its own lane with time. Then, we discuss the estimation of the geometry of the lane that gives information about the curvature of the road, and finally, we investigate the presence of adjacent lanes, which is a feature that is not typically treated in the related literature.

5.1 Lane tracker

The lane tracker technique is commonly known as the functionality of an ADAS system that analyzes the evolution of the images and determines the width of the own lane, w_k, and the position of the vehicle within it, x_k. Hence, lane changes are also detected by analyzing the evolution of x_k and w_k.

This evolution is easily described as a dynamic linear system that can be solved with a Kalman filter defined by the following state-space equation:

$$\mathbf{x}_k = \mathrm{A}\mathbf{x}_{k-1} + \mathrm{B}\mathbf{u}_k + \mathbf{n}_k \tag{11}$$

where the state vector is $\mathbf{x}_k = (x_k, w_k, \dot{x}_k, \dot{w}_k)^\top$. The measurement vector is, at each instant, $\mathbf{z}_k = (x_k, w_k)^\top$, which is the instantaneous measurement of the target parameters. The following paragraphs explain how these measurements are extracted. The transition matrix, A, and the input control matrix, B, are given by a constant-velocity model. The use of this model does not mean that we assume a constant velocity over all time; rather, the statistical model of the motion assumes undetermined accelerations with a Gaussian profile, modeled by $\mathbf{n}_k$.

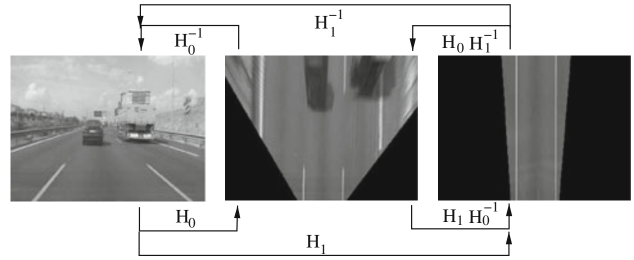

Fig. 12 Image-plane to road plane transforms: H_0 image-plane to road-plane; H_1 image-plane to zoomed road-plane

The control matrix, $B = (1, 0, 0, 0)^\top$, is used to modify the estimation of the transversal position of the vehicle when lane changes are detected. The input control vector is obtained as

$$\mathbf{u}_k = \begin{cases} w_k & \text{if } x_k > \frac{1}{2}(W + w_k) \\ -w_k & \text{if } x_k < \frac{1}{2}(W - w_k) \end{cases} \tag{12}$$

where W is the width of the image in pixels; hence, when the transversal position exceeds the boundary, at the left or right, of the estimated lane, the input control is activated and the transversal position is shifted.

The measurement vector, $\mathbf{z}_k$, is obtained by recomputing the transformed domain. Namely, a new zoomed road-plane image that contains information regarding a very near stretch of the road is created. Figure 12 shows the relationship between the image plane, the road plane, and this new zoomed road plane. As shown, the zoomed road plane contains only the very lower part of the original image plane in order to avoid the presence of vehicles. Within this zoomed image, only the lane markings that belong to the own lane are displayed and lane markings can be modeled by straight lines.

The measurement vector is obtained using the Hough transform on the segmented zoomed road plane. Two straight lines model the two lane markings of the own lane. These lines intersect the bottom boundary of the image in two points. The distance between these points is the measurement w_k, while the difference between their middle point and the mid-lower point of the image is x_k.

The tracking process of the own vehicle position is depicted in Fig. 13. As shown, the noisy measurements are smoothed with the Kalman filter, which also allows the prediction and correct detection of the lane change event.

5.2 Lane modeling

In this section we discuss the process of modeling the own lane. This is done by selecting a set of control points of the lane along the transformed image and then fitting a pair of curves (one for each lane marking of the lane) using these control points.

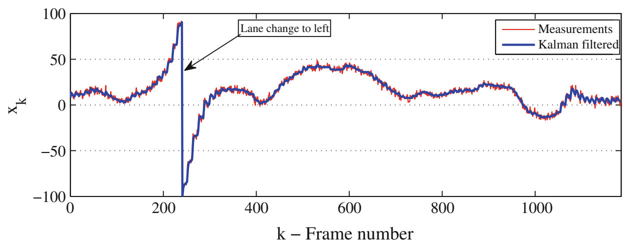

Fig. 13 Estimation of the transversal position of the own-vehicle inside its lane (varying from 100 to −100% corresponding to the left-most and right-most position inside the lane)

5.2.1 Control points generation

Given the segmentation of the image, in this stage we compute the *control points*, defined by their 2D positions, $\mathbf{x}_k^i$, which give enough information to model the geometry of the lane. The detection of the control points is carried out such that they are distributed throughout the whole image and constitute a quasi-regular grid, which is updated dynamically along time. This detection then allows for a better and easier estimation of the curve that best fits them.

For each frame, the control points are updated as shown in Fig. 14, using their previously computed position and the set of new measurements obtained from the pixels that belong to lane markings. The measured control points are compared with the grid formed by the previous set of control points, depicted with circles in Fig 14c. These measurements are clustered around the previous control points, i.e., $\{\mathbf{x}_{k-1}^i\}_{i=1}^{N_0}$, so that each previous control point has an associated set of M_i measures, $\{\mathbf{z}_k^{i,j}\}_{j=1}^{M_i}$, which are closer to it than to any other control point. Therefore, the estimation of the control points depends on the number of measurements that fall inside its corresponding cell. The estimated value is computed as

$$\mathbf{x}_k^i = \begin{cases} \mathbf{x}_{k-1}^i & \text{if } M_i = 0 \\ \mathbf{z}_k^i & \text{if } M_i = 1 \\ \mathbf{z}_k^{i,*} & \text{elsewhere} \end{cases} \tag{13}$$

where $\mathbf{z}_k^{i,*}$ is the measure with the smaller distance to the previous control point:

$$\mathbf{z}_k^{i,*} = \min_{\mathbf{z}_k^{i,j}}\{\|\mathbf{x}_{k-1}^i - \mathbf{z}_k^{i,j}\|\} \tag{14}$$

5.2.2 Curve fitting

The complexity of the curve modeling of each lane marking increases as the number of control points being considered increases. The number of control points per lane marking, c, models different curve types. If $c = 2$, the model may be a line [25,26]; $c = 3$ defines generic second-order curves, such as parabolas [11,27], circles, and constrained cubic curves

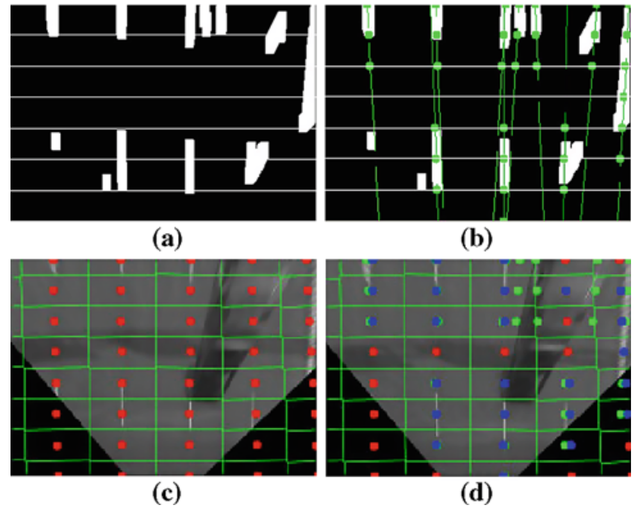

Fig. 14 Measurement generation: **a** blobs from dilated lane marking pixels; **b** intersection of Hough lines from each blob with horizontal lines; **c** previous image with its Voronoi cells division in *solid lines*, and the set of points $\mathbf{x}_{k-1}^i$ in *circles*; **d** current image with measured $\mathbf{z}_k^{i,j}$; estimated $\mathbf{z}_k^{i,*}$; and predictions $\mathbf{x}_{k-1}^i$

approximating clothoids [12], while for $c = 4$, more complex spline shapes [13] can be estimated.

Typical approaches use parabolic models [11] for lane modeling, which offer enough accuracy for both transformed domain and original images. However, for the transformed images, generic circumference arc models show better performance in most situations.

Some researchers use the maximum likelihood method [26,27] to estimate the parameters of these models. However, RANSAC is preferred here as it is a robust estimation approach that shows much better performance by removing outliers from the set of points [22].

For better performance, we assume that the circumference center is at some point on the horizontal line defined by $y = H$, i.e., the bottom row of the image. This assumption forces the vertical to be tangent to the circumference in the lower part of the image, which is in line with the assumption that the vehicle is moving approximately parallel to the lane markings.

Figure 15 shows an example of curve fitting assuming a circumference model on the rectified domain. Note that the curvature is moderate in this type of motorways scenario such that the circumference model achieves a good trade-off between accuracy and simplicity.

5.3 Multiple lanes estimation

Once the own lane has been estimated in terms of position and geometry, the presence of adjacent lanes is hypothesized by assuming that these lanes have the same geometry and width, i.e., they are located at w_k pixels at left and right.

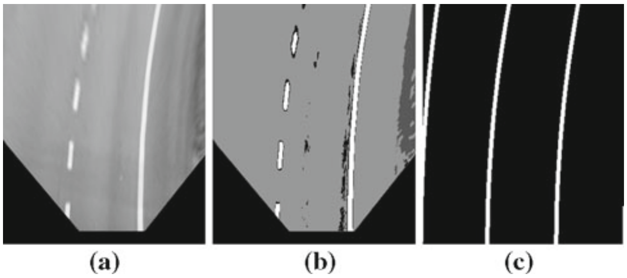

Fig. 15 Curve fitting for an example image: **a** rectified image; **b** segmentation after Bayesian classifier; and **c** the resulting circumference model

Several adjacent lanes may be also hypothesized this way, considering a model defined by the parameter vector $(x_0, y_0, r \pm n \cdot w_k)^\top$ where n indexes the number of hypothesized lanes at left or right.

The verification of adjacent lanes is performed by checking the percentage of pavement pixels contained at each hypothesized lane. The probability that a hypothesized lane, indexed by l, actually exists is given by

$$P_l = \frac{1}{N} \sum_{\{xy\} \in l} P(X_p | \mathbf{z}_{xy}) \tag{15}$$

where the summation is carried out only for the pixels within the hypothesized lane, whose cardinality is N. The same statistic is computed for the "unknown" and "Lane marking" classes. Therefore, it is straightforward to determine the presence of a lane if P_l is greater than these statistics.

6 Vehicle detection and tracking

The strategy proposed for vehicle detection and tracking lies on the basis of a previous object segmentation in the transformed image. The proposed framework is flexible as it can operate over an arbitrary segmentation technique. Particularly, for this work the segmentation explained in Sect. 4 is used due to its efficiency and reliability. Based on this segmentation, the method achieves vehicle detection and tracking by exploiting geometric and appearance information of the objects. It involves a collaborative analysis of the original and the transformed images. The former gives a complete view of the scenario ahead of the vehicle, but the information content is not homogeneously distributed among the pixels due to the perspective effect [28]. The latter, in turn, removes non-linearity at the expense of losing detail during the transformation.

First, vehicle detection is addressed by analyzing the segmentation image in the transformed domain. Vehicle candidates are extracted using the geometric information of the objects in this domain (i.e., the effect of the homography over a volumetric object in the perspective image) and the properties of the bird's-eye view. On the other hand, the domain duality allows to verify the compliance of the measured candidates with the expected appearance of vehicles in the original domain.

Additionally, vehicle tracking is obtained by associating the measurements at different instants, so that the track of each vehicle can be identified. The method comprises as well new vehicle management based on the spatial and temporal coherence of the measurements. Note that the transformed domain highly simplifies data association, as vehicles positions and velocities are proportional to the corresponding actual magnitudes. Conversely, the original image allows to refine tracking results, both in the position and the dimension of the vehicles, which again supports the convenience of the proposed dual domain approach. Finally, coherent results in time are ensured by introducing the measurements in a probabilistic framework governed by a Kalman filter. This framework enables us as well to make predictions of the vehicles positions in the following times. This is especially useful as it allows to maximize the information exchange between the segmentation process and the vehicle detection stage. Namely, a feedback loop is created in which the Bayesian segmentation framework receives theses predictions as prior probabilities.

6.1 Measurement generation

As stated, measurements for vehicle detection are extracted from the dual domain analysis based on the segmentation explained in Sect. 4. The regions of the image segmented as objects are taken into account at this stage. Note that all vehicles contain a dark area in their lower part due to shadow and wheels, which will be classified as object. This dark part is enlarged in the transformed domain, as shown for the white vehicle in Fig. 8b). However, this segmentation is performed at a pixel level; hence, the result often shows unconnected regions and is corrupted by noise (see Fig. 16b, where the pixels belonging to the object class are painted in white). Therefore, a morphological opening operation, i.e., an erosion followed by a dilation, is performed to obtain enhanced images in which objects are clearly segmented. The initial erosion (typically involving a small square structuring element) removes background noise, whereas the subsequent complementary dilation operation restores the contours of the objects, as shown in Fig. 16c, d, respectively.

As a result of these operations, an enhanced image is obtained, which consists of several compact white zones (known as blobs). These blobs, characterized by their position, $\mathbf{x}$, and width, w, as illustrated in Fig. 16e, represent the hypotheses for the vehicles in the image. The verification of these hypotheses is performed twofold. First, the nature of the underlying projectivity to the road-plane is taken into account. Namely, the homography produces a

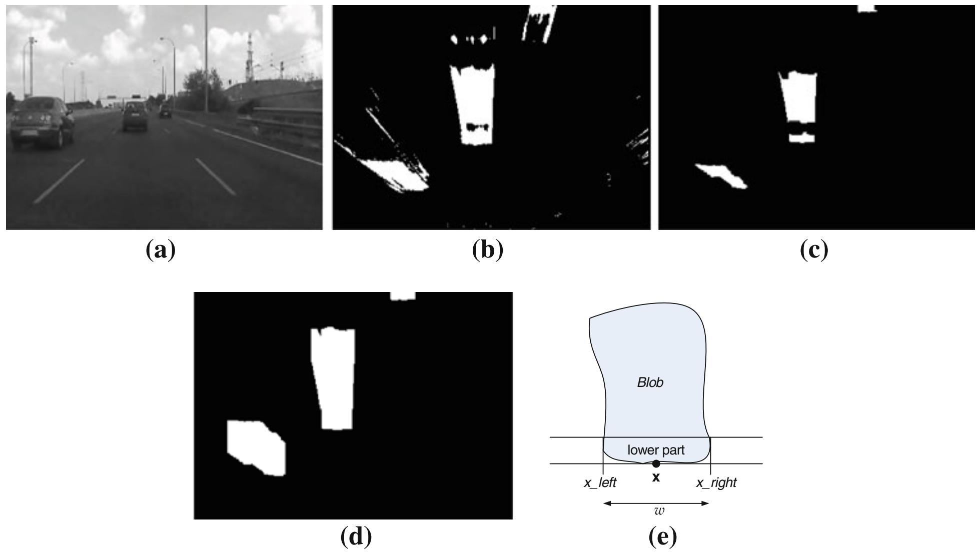

Fig. 16 Image in **b** shows the segmentation of **a**. **c**, **d** Correspond to the erosion of **b** and dilation of **c**, respectively. A typical blob is shown in **e**, where only the lower part is taken into account due to perspective distortion

radial distortion of the elements of the objects above the road plane, as can be observed in Fig. 2. Hence, only the candidates showing a shape compliant with this kind of distortion are considered. Observe that in the example in Fig. 16d both candidates have the expected shape.

On the other hand, the dual domain approach allows to check the appearance of the hypothesized vehicles in the original domain. The inverse homography H^{-1} delivers the position and width of the candidates in this domain. Additionally, assuming a standard aspect ratio of vehicles (i.e., 1.2:1) a rectangular region is defined around each hypothesized vehicle position. The verification is performed in these regions, and is based on different cues for close and distant objects. For the former, a symmetry measure is used, since the rears of vehicles have a high degree of symmetry around the vertical axis. Hence, the vertical symmetry, denoted f and normalized between 0 and 1, is computed as in [17] inside the bounding box. Regions with high symmetry values ($f > t_f$) are classified as potential vehicles. As for distant vehicles, the resolution is usually not sufficient to provide a significant symmetry value. In this case, the edge density is used as a cue for vehicle verification. Vehicles present a high density of edges owing to their contrast with the background, plate, back glass, etc. Hence, the edge density is computed in the hypothesized window as

$$d = \frac{1}{R_x R_y} \sum_{x,y \epsilon R} e(x, y) \tag{16}$$

where $e(x, y)$ is the edge intensity of pixel (x, y) between 0 and 1 computed using the Sobel edge detector, and R is the bounding box of the candidate, with dimensions $R_x \times R_y$. Candidates with high edge density values ($d > t_d$) are classified as potential vehicles. The thresholds t_f and t_d are defined in such a way that the negative classification of true vehicles is minimized, even if it involves some false detection. These can be effectively filtered in the tracking stage due to their lack of coherence and persistence, as explained below.

6.2 Vehicle tracking

The segmentation provides instantaneous measurements of the positions of the vehicles. However, valuable insight in the characterization of the vehicles (position, trajectory, new vehicle entries, etc.) can be attained by analyzing the temporal evolution of these measurements. Remarkably, the transformed domain constitutes a suitable framework to perform temporal correlation: in effect, it provides an up-to-scale reconstruction of the road plane and thus data association can be performed on the basis of Euclidean distances. This largely simplifies as well vehicle entry and exit management. Additionally, in the transformed domain motion of vehicles is proportional to their true motion; thus it can be modeled via a linear process based on Kalman filtering. On the other hand, the lack of accuracy and of height information inherent to this domain are compensated by resorting to the original domain, which is richer in details and hence provide refined data.

6.2.1 Data association

Note that at each instant independent results are obtained for the set of vehicles. In addition, occasionally some false positives or negatives can occur as a result of poor segmentation of the objects. Therefore, data association between frames is needed. The objective is to assign n measures in the current frame to m existing vehicles. In this work, a clustering technique based on a similarity criterion is applied. Namely, a similarity function is defined that compares the attributes

Fig. 17 Examples of the applied clustering technique. Predicted vehicles are painted with a *solid line* and a *cross* in the middle (the *cross* indicates position $\mathbf{x}_p$, and the segment corresponds to width w_p), and blobs associated with them are patined as isolated crosses

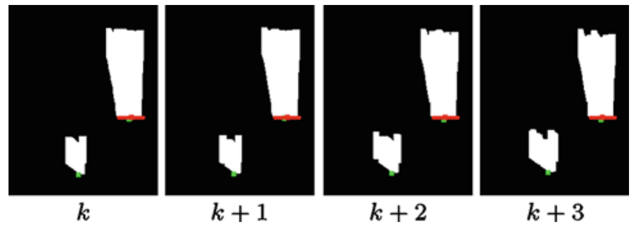

Fig. 18 New object management. At time k, a new blob appears in the image, which already contains one existing vehicle. The new blob fulfills both spatial and temporal coherence criteria at times $k+1$, $k+2$ and $k+3$; thus, it is classified as a vehicle and tracked henceforth

of each current candidate, $(\mathbf{x}_c, w_c)$, with those predicted for each vehicle, $(\mathbf{x}_p, w_p)$. The *similarity* is modeled as a function of two factors relating to the relative position and the relative width of the candidates as

$$S = \frac{w_p}{|w_p - w_c|} \frac{1}{\|\mathbf{x}_p - \mathbf{x}_c\|} \tag{17}$$

The distance is defined as a Euclidean metric, and it considers the mid-lower pixel of the blob as defined in Fig. 16e. Naturally, the blob that maximizes the similarity function for each vehicle is assigned to it. Clustering is illustrated in Fig. 17 with two examples, in which the predictions are shown with line segments with a cross in the middle, and the attributes of the candidates most *similar* to them are painted as isolated crosses. In Fig. 17a, five blobs are segmented and only three vehicles are predicted; the assignment is clear as the position and width of the selected blobs are very similar to the predictions. In Fig. 17b, three blobs are found for two predicted vehicles. Here, for the lower predicted vehicle, the larger blob is selected although the small blob in the left is slightly closer to the prediction, due to its similarity in the width. Finally, if no measurement is found for the vehicle, the tracking process relies on the predicted attributes associated with it. This reveals the suitability of the predictive nature of the proposed framework.

6.2.2 New vehicle management

The above method relates existing vehicles with their corresponding new measurements. However, new vehicles may enter the scene at time k. These appear as additional blobs in the enhanced segmentation image. On the other hand, some spurious blobs may also arise due to artifacts in the segmentation. A twofold verification (i.e. spatial and temporal) is carried out to differentiate the blobs corresponding to entering vehicles. First, due to kinetic constraints between consecutive frames, vehicles may only appear in the uppermost (far vehicles coming closer) or lowermost (vehicles overtaking the own vehicle) zones of the road-plane image. Hence, to ensure spatial coherence, only these zones are analyzed.

Additionally, a temporal coherence criterion is enforced for the remaining blobs, i.e., a set of *similar* blobs is sought in the following frames (see Fig. 18). The similarity function is evaluated for every set according to the descriptor in (17). Eventually, a new vehicle is hypothesized when the elements of the set fulfill the similarity condition $S > 2/t_d$. Visually, this condition holds if, after the initial observation of the blob at time k, a blob is found at subsequent time points that is inside the search area of radius t_d ($\|\mathbf{x}_p - \mathbf{x}_c\| < t_d$) and has a width at maximum of 50% larger or smaller than the initial observation ($\frac{|w_p - w_c|}{w_p} = 1/2$). This is the case for the example in Fig. 18, where the position and width of the detected new blob are similar throughout four consecutive frames. Note that both the spatial and the temporal verification are widely simplified due to operation in the homogeneous transformed domain, as opposed to classical approaches working in the original domain, which usually require more complex analysis or additional a priori conditions.

6.2.3 Detection refinement

Results obtained in the transformed domain provide a coarse approximation to ground truth, as the change of domain entails a certain loss of accuracy. In addition, the transformed domain involves a bird's-eye view and thus removes information regarding the height dimension of the vehicles. The proposed collaborative approach is exploited here to shift the processing to the original domain. The objective is twofold: (i) to refine the widths and positions obtained in the transformed domain, and (ii) to allow the estimation of the height of the vehicles in order to provide a more complete characterization.

Refinement in the original image is based on edge information; in effect, the contour of the vehicle rear usually presents abrupt edges. Hence, edge information is used to refine the bounding box of each vehicle. The rectangle bounding the vehicle is obtained using the inverse homography H^{-1} in the same manner as in Sect. 6.1. In order to ensure that edges are contained in it, the region is expanded around the hypothesized bounding box, and the Sobel edge detector is applied

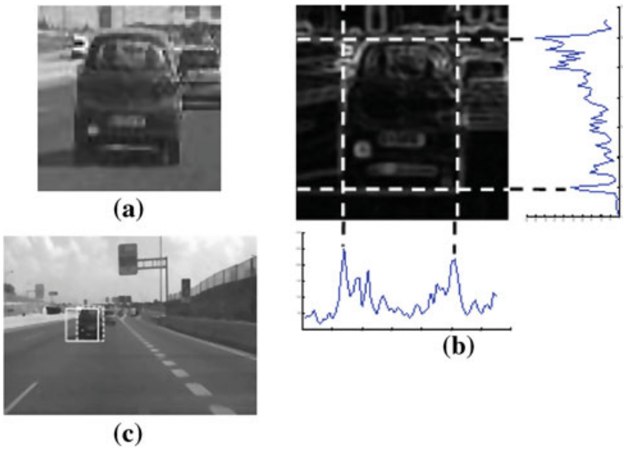

Fig. 19 Vehicle detection refinement: **a** A detail of the closer vehicle in **c**; **b** is the result of Sobel operator over **a**. Observe that both the vertical and the horizontal edge histograms feature prominent peaks in the positions of the vehicle contour

over all of the pixels in the extended region. This is illustrated in Fig. 19: the image in b corresponds to the edge intensities computed over the image in a, which in turn shows a detail of the closest vehicle in c. Then, the resultant edge sub-image in b is scanned and the values are added up, first left to right to produce the horizontal edge histogram, and, in turn, bottom to up to render the vertical edge histogram (see Fig. 19b). The former is expected to have prominent peaks for the upper and lower limits of the vehicle, while the second will contain two peaks, for its left and right limits. The local maxima are selected at each side of the histogram so that a refined bounding that fits the real contour of the vehicle box is finally obtained. The achieved fine-tuning is illustrated in Fig. 19c, where the solid line depicts the coarse detection obtained from the transformed domain, and the dotted line corresponds to the refined bounding box. As a result of this stage, height information is added to the previous vehicle attributes, position and width, which are in turn fine-tuned.

6.2.4 Probabilistic filtering

So far, the method obtains sequential measurements for each of the vehicles in the scene. These measurements are time-correlated (i.e., a track is kept for each vehicle) but lack coherence in what concerns their fitting the known dynamics of vehicles. In effect, vehicles move forward with a locally uniform pace, especially in highways. Therefore, smooth changes are expected in the position of the vehicles on the road and their velocity is approximately constant, at least locally. This knowledge allows to introduce the measurements into a probabilistic framework that filters noisy instantaneous measurements, thus providing smooth results. In particular, in the transformed domain vehicle dynamics are proportional to their actual magnitudes; hence the state evolution in this domain can be considered to be linear. Therefore, the transformed domain enables us to model vehicle kinetics with a constant-velocity Kalman filter.

The state vector is composed of the position (x, y), velocity $(\dot{x}, \dot{y})$, width (w), and normalized height $(\bar{h})$ of an object:

$$\mathbf{x}_k = (x, y, \dot{x}, \dot{y}, w, \bar{h})^\top \tag{18}$$

For every time point k, the object attributes (position, width and height) are measured; thus, the measurement vector $\mathbf{z}_k$ is given by

$$\mathbf{z}_k = (x, y, w, \bar{h})^\top \tag{19}$$

Both the position and width measurements refer to the road-plane image, where the linearity condition holds. Hence, these measurements must be transformed back to the original image after the refinement stage. Conversely, the height information only exists in the original image, where it is non-linear due to perspective. To make it linear, a normalized height measure, $\bar{h}$, is defined as in [29].

As regards the choice of the process and measurement noise covariance, the following considerations are insightful. First, the process noise must be low due to the adequacy of the linear evolution of the state vector for a real scenario. In particular, the noise covariances of the width and height attributes are almost zero, as the dimensions of the object are actually constant. As for the measurement noise, the uncertainty is larger as it depends on the accuracy of the segmentation. In any case, its covariance should be larger that of the process noise in order to prevent the system from being corrupted by poor measurements. Noise covariances may be tuned to adapt more quickly to changes in the measurements or to enforce smoothness, as long as the process noise remains smaller than the measurement noise.

Note that the predictive nature of the Kalman filter is of great value as it allows to create a feedback loop which enriches other stages of the system. Indeed, predictions are used to perform data association on the incoming measurements (see Sect. 6.2.1). Moreover, they are also used to feed back the segmentation process, namely the expected positions of the vehicles are used to define the prior probability to belong to the object class. In effect, since the vehicle position and width estimates are available, and given the radial distortion produced by the road plane homography, it is possible to infer the regions potentially containing objects in the following frame. In this work, a binary probability map is generated as shown in Fig. 11b. This feedback loop allows to maximize data exchange between modules and thus to capitalize on all available information.

7 Tests and discussion

All the developments have been carried out in C++ programming language, under an MFC solution for Windows and Direct Show primitives. This architecture allows for a real-time performance of the system for real on-road operation as well as continuous visualization of the processed data. Moreover, the system was designed to be able to acquire the video stream from different digital interfaces, such as USB, FireWire, GEthernet, etc. Nevertheless, for the trials, the acquiring system was composed of a forward looking digital video camera SONY HDR-HCR5E, installed near the rear mirror, and a FireWire connection to the processing system. The size of the images is 360×288, which allows the system to work near real-time, at 15 frames per second on average (including video visualization and output data generation) in a laptop Core2Duo at 2.2 GHz with 2 GB of RAM.

The real on-road trials have been conducted in different roads in Madrid, Brussels, Milano, Torino, and the A4 Brescia–Padova motorway (during the test sessions carried out in different stages of the I-WAY integration activities). From these trials, we have collected a large number of sequences (with a total length of around 150 min) from which we have gathered relevant output data. The target is to analyze the behavior and the performance of the system, monitoring its main output parameters, namely, the position of the vehicle inside its lane, the number of lane changes, the curvature, the positions of the vehicles ahead, and their dimensions.

Different scenarios are considered to demonstrate the ability of the system to adapt to the uncontrolled outdoor scenario, including changing illumination conditions, different pavement color, varied weather conditions, different type of lane markings, presence of vehicles that cause occlusions, etc. Attending to the results obtained through the tests, we can extract the following conclusions:

The position of the own vehicle inside its lane (a feature that depends on the lane tracker performance, described in Sect. 5.1) is estimated with high accuracy in almost all situations. Some examples are shown in Fig. 20. The central overlaid region defines the closer part of the own lane, according to the detected lane markings, depicted with thick solid lines. The center of the lane is marked with a thin solid line, and the center of the image with a shorter black line. The relative position of the vehicle in the lane is depicted with a numerical indicator, which is 0% at the center of the lane, and -100 and 100% at its left-most and right-most position, respectively. As shown, the width of the lane may vary, but it is accurately estimated by the system.

The lane change detection is one of the higher performance features of the developed system (as will be shown in Table 1). The second row of Fig. 20 shows some detected lane changes, whose direction is indicated with a superimposed icon. The detection of the significant curves depends on the visibility of the lane markings in the far distance, which is generally good provided that the traffic load is not too heavy. In these situations, the system correctly detects the curvature, as in the examples shown in the third row of Fig. 20.

Regarding the detection of multiple lanes, the system has shown excellent performance in most situations. As long as the segmentation result is correct, which is true for most situations, the system is able to hypothesize the presence of adjacent lanes to the own lane and confirm their presence using the Bayesian segmentation information. Different examples illustrate this ability in the Fig. 20: when driving in the right lane, the system is able to determine that there are no more lanes at the right, and analogously when driving in the left-most lane. When driving in the central lanes, three lanes are hypothesized at most. This number is not a limitation of the algorithm, but a design parameter, as beyond these there are not enough pixels to take a reliable decision.

In the field of vehicles detection, most of the cars are correctly detected in the region of interest (up to 35 m inside the detected lanes) for all the considered scenarios. The Fig. 20 shows several examples of detected vehicles, represented by a rectangular box around these, that illustrate the dimensions of the vehicles, as well as their location inside the lanes. Provided that the camera is calibrated, its distance in meters to the camera is printed with a yellow numerical indicator. First, recall that the dimensions of the vehicles are typically well estimated, up to some errors due to the presence of intense edges at the background. Second, the tracking framework allows to keep track of the vehicles, giving a temporal coherence to the detection, as well as robustness against brief occlusions, such as the one shown in the two last images of Fig. 20. This is a raining scene, where even with the presence of the wipers, which appear and occlude the vehicle momentarily, the tracker succeeds in maintaining the detection of the vehicle for successive frames.

One of the major abilities of the proposed system is its demonstrated robustness against challenging, unpredictable situations. On-road trials feature, for instance, sudden illumination changes (e.g. when entering into tunnels, or passing below a bridge), the appearance of the aforementioned elements such as wipers, drawings on the road, drops on the windscreen, irregular color of the pavement, reflections, etc. The proposed models rely on the robustness of the probabilistic segmentation, that is able to handle any of these difficulties with the "unknown" class. In few words, the system has been designed to search for and model lane markings, the color of the pavement and vehicles, and to not be deceived by this type of uncontrolled scenarios.

Figure 20 show the excellent performance of the system for a wide variety of scenarios. In order to reflect more objectively the performance, a set of relevant parameters has been defined, i.e., vehicle detection rate (VDR), lane change detection rate (LCDR), vehicle false positive rate (VFPR),

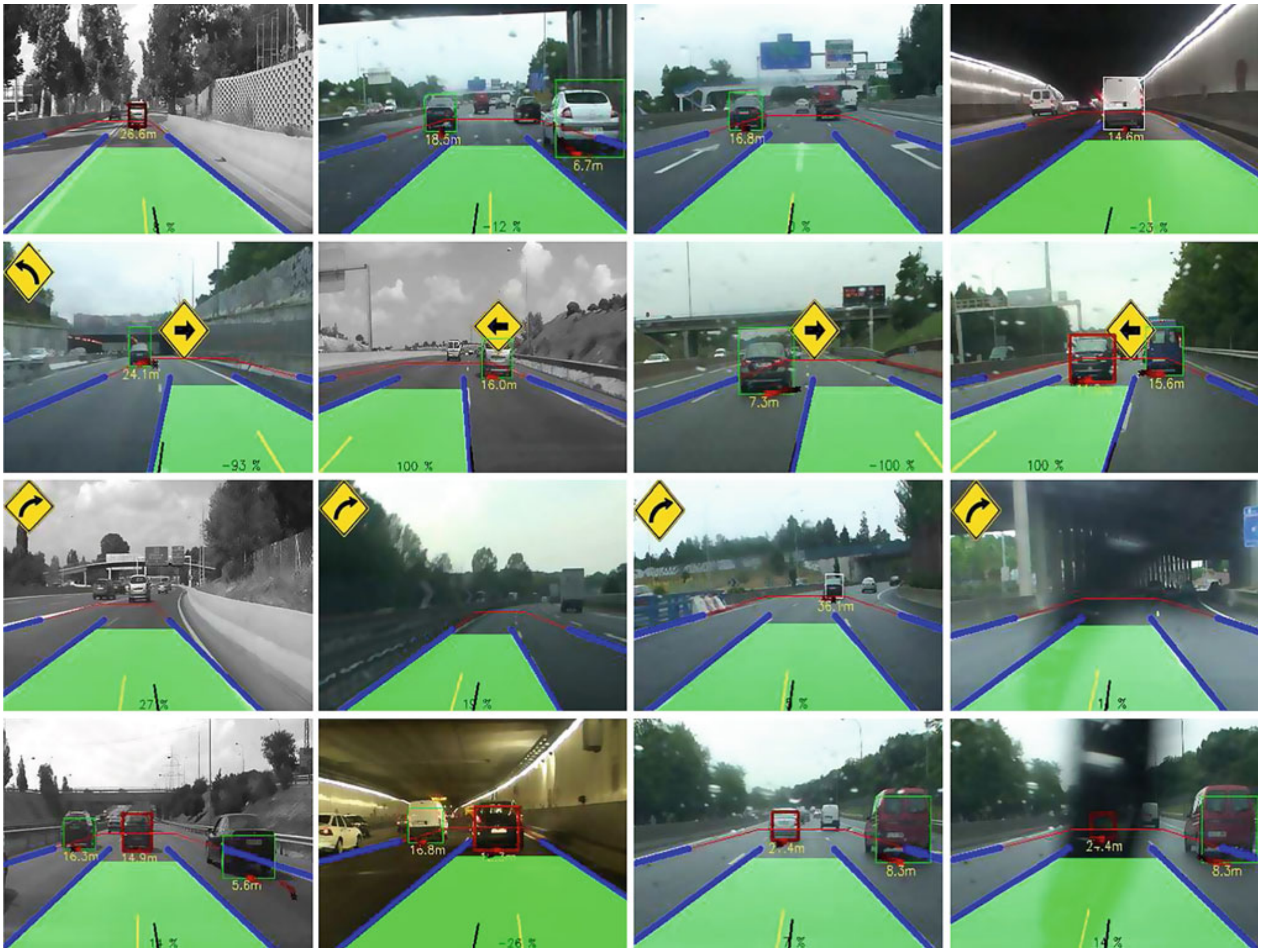

Fig. 20 Examples showing the detected elements of the road: In the *upper row* some representative examples of the accuracy of the lane tracker are shown; the *second row* shows examples of lane change events; and the *lower row* illustrates vehicle detected in difficult scenarios

Table 1 Detection results for different scenarios

Event	Type of scenario	
	Typical	Complex
No. of total vehicles	1,056	1,177
No. of detected vehicles	1,021	1,079
No. of lane changes	204	211
No. of detected lane changes	196	197
No. of false positive vehicles	21	46
No. of false positive lane changes	3	9
VDR (%)	96.69	91.67
LCDR (%)	96.08	93.36
VFPR (%)	1.98	3.90
LCFPR (%)	1.47	4.27

and lane change false positive rate (LCFPR). The former two are defined as the number of correct detections over the total number of events (presence of vehicle or lane change, respectively) indicated by the ground truth. The latter are defined analogously as the number of false positives. They have been measured off-line for a large set of sequences corresponding to two scenarios: typical and complex. The former involves the typical driving conditions in motorways, that is, well-painted lane markings, variable illumination conditions with soft changes, low/medium traffic density, or favorable weather conditions (including mild rain). The latter comprises those conditions that are not so commonly encountered in motorways (such as dense traffic or variable illumination conditions with rapid and abrupt variations), or those that occur for short periods of time (such as tunnels, which entail artificial illumination conditions).

Table 1 shows the performance of the system, in terms of detection and false positive rates, for the two sets of scenarios. As can be observed, the vehicle detection and the lane change detection rates are very high (over 96%) in a typical scenario. In this situation, the false positive rate is under 2% for both features. As for complex scenarios, the vehicle detection rate decreases to 91.67% and the lane change detection rate to 93.36%. Both figures are reduced but still show excellent performance, the higher impact in the former being due to the complexity of the shadow analysis in this kind of scenarios and to the occlusions between vehicles when dense traffic load exists.

8 Conclusions

In this paper a novel vision-based road environment modeling is proposed, which comprises a model of the lanes, as well as the situation of the own vehicle and others in the road. The proposed solution entails a number of innovative techniques, which separately address the different stages of the processing (stabilized road plane rectification, adaptive Bayesian segmentation and temporal coherent models for lane marking detection and vehicle detection and tracking) and whose combination results in a system that is robust, adaptive, and accurate. One of the main advantages of the proposed strategy is its robustness against the uncontrolled changing conditions of the road environment: the illumination may vary dramatically in few frames (consider the entrance to a tunnel), the weather may introduce artifacts in the image such as those produced by the wipers, variation in the color of the pavement of the road (in terms of its homogeneity and its contrast to other elements, such as lane markings or vehicles), and presence of different type of vehicles. The information provided by this system is of great interest for decision systems, as it includes the position of the vehicle inside its own lane, the width of the lane, the presence of adjacent lanes, the relative position and motion of other vehicles in the road, as well as their dimensions. The system has been tested on-road for a wide variety of situations, resulting in all cases in excellent performance.

Acknowledgments This work has been partially supported by the Ministerio de Ciencia e Innovación of the Spanish Government under project TEC2007-67764 (SmartVIsion), and by the European Commission 6th Framework Program under project IST-2004-027195 (I-WAY).

References

1. Sun, Z., Bebis, G., Miller, R.: On-road Vehicle Detection Using Optical Sensors: A review. In: IEEE Proc. Int. Conf. on Intelligent Transportation Systems, pp. 585–590 (2004)
2. Bertozzi, M., Broggi, A.: GOLD: A parallel real-time stereo vision system for generic obstacle and lane detection. IEEE Trans. Image Process. **7**(1), 62–81 (1998)
3. Nedevschi, S., Schmidt, R., Graf, T., Danescu, R., Frentiu, D., Marita, T., Oniga, F., Pocol, C.: 3D Lane Detection System Based on Stereovision. In: IEEE Proc. Intelligent Transportation Systems Conference, pp. 161–166 (2004)
4. Nedevschi, S., Oniga, F., Danescu, R.: Increased Accuracy Stereo Approach for 3D Lane Detection. In: IEEE Proc. Intelligent Vehicles Symposium, pp. 42–49 (2006)
5. Danescu, R., Nedevschi, S., Meinecke, M.-M., To, T.-B.: A Stereovision-Based Probabilistic Lane Tracker for Difficult Road Scenarios. In: IEEE Proc. Intelligent Vehicles Symposium, pp. 536–541 (2008)
6. Broggi, A., Bertozzi, M., Fascioli, A.: Self-calibration of a Stereo Vision System for Automotive Applications. In: IEEE Proc. Int. Conf. on Robotics and Automation, vol. 4, pp. 3698–3703 (2001)
7. Chang, P., Hirvonen, D., Camus, T., Southall, B.: Stereo-Based Object Detection, Classification, and Quantitative Evaluation with Automotive Applications. In: IEEE Proc Computer Vision and Pattern Recognition, vol. 3, pp. 62–68 (2005)
8. Simond, N., Rives, P.: Homography from a vanishing point in urban scenes. In: IEEE/RSJ Int. Conf. on Intelligent Robots and Systems, vol. 1, pp. 1005–1010 (2003)
9. Stein, G.P., Mano, O., Shashua, A.: A Robust Method for Computing Vehicle Ego-motion. In: IEEE Proc. Intelligent Vehicles Symposium, pp. 362–368 (2000)
10. Zhou, J., Li, B.: Homography-based Ground Detection for A Mobile Robot Platform Using a Single Camera. In: IEEE International Conference on Robotics and Automation, pp. 4100–4105 (2006)
11. McCall, J.C., Trivedi, M.M.: Video-based lane estimation and tracking for driver assistance: Survey, system, and evaluation. IEEE Trans. Intell. Transport. Syst. **7**(1), 20–37 (2006)
12. Corridori, C., Zanin, M.: High curvature Two-Clothoid Road Model Estimation. In: IEEE Intelligent Transportation Systems Conference, pp. 630–636 (2004)
13. Wang, Y., Teoh, E.K., Shen, D.: Lane detection, tracking using B-snakes. Image Vision Comput. **22**, 269–289 (2004)
14. Chen, Y., Das, M., Bajpai, D.: Vehicle Tracking and Distance Estimation Based on Multiple Image Features. In: IEEE Proc. Canadian Conf. on Computer and Robot Vision, pp. 371–378 (2007)
15. Goecke, R., Pettersson, N., Petersson, L.: Towards Detection and Tracking of On-Road Objects. In: IEEE Proc. Intelligent Vehicles Symposium, pp. 416–421 (2007)
16. ten Kate, T.K., et al.: Mid-range and Distant Vehicle Detection with a Mobile Camera. In: IEEE Proc. Intelligent Vehicle Symposium, pp. 72–77 (2004)
17. Hoffmann, C., Dang, T., Stiller, C.: Vehicle detection fusing 2D visual features. In: IEEE Proc. Intelligent Vehicle Symposium, pp. 280–285 (2004)
18. Jiang, G.Y.: Lane and Obstacle Detection Based on Fast Inverse per spective mapping algorithm. In: IEEE Proc. Int. Conf. on Systems, Man, and Cybernetics, vol. 4, pp. 2969–2974 (2004)
19. Shu, Y., Tan, Z.: Vision Based Lane Detection in Autonomous Vehicle, In: Proc. 5 World Congress on Intelligent Control and Automation, pp. 5258–5260 (2004)
20. Nieto, M., Salgado, L., Jaureguizar, F., Cabrera, J.: Stabilization of Inverse Perspective Mapping Images based on Robust Vanishing Point Estimation. In: IEEE Proc. Intelligent Vehicles Symposium, pp. 315–320 (2007)
21. Mallot, H., Bulthoff, H., Little, J., Bohrer, S.: Inverse perspective mapping simplifies optical flow computation and obstacle detection. Biol. Cybern. **64**(3), 177–185 (1991)
22. Hartley, R.I., Zisserman, A.: Multiple View Geometry in Computer Vision, Second. Cambridge University Press, Cambridge (2004)
23. Macek, K., Williams, B., Kolski, S., Siegwart, R.: A Lane Detection Vision Module for Driver Assistance. In: IEEE Proc. Conf. on Mech. and Robotics, pp. 77–82 (2004)
24. Bilmes, J.A.: A Gentle Tutorial on the EM Algorithm and its Application to Parameter Estimation for Gaussian Mixture and Hidden Markov Models. http://citeseer.ist.psu.edu/bilmes98gentle.html, technical report, Univ. of California, Berkeley (1998)
25. Kang, D.-J., Jung, M.-H.: Road lane segmentation using dynamic programming for active safety vehicles. Pattern Recognit. Lett. **24**(16), 3177–3185 (2006)

26. Kaliyaperumal, K., Lakshmanan, S., Kluge, K.: An algorithm for detecting roads and obstacles in radar images. IEEE Trans. Vehicular Technol. **50**(1), 170–182 (2001)
27. Kluge, K., Lakshmanan, S.: A deformable-template approach to lane detection. In: IEEE Proc. Intelligent Vehicles Symposium, pp. 54–59 (1995)
28. Bertozzi, M., Broggi, A., Fascioli, A., Fascioli, R.: Stereo inverse perspective mapping: theory and applications, image and vision. Comput. J. **8**, 585–590 (1998)
29. Arróspide, J., Salgado, L., Nieto, M., Jaureguizar, F.: Real-Time Vehicle Detection and Tracking Based on Perspective and Non-Perspective Space Cooperation. In: IST/SPIE Proc. Int. Conf. on Real-Time Image and Video Processing, vol. 7244, pp. 72440H-1-12 (2009)
30. Cerri, P., Grisleri, P.: Free Space Detection on Highways using Time Correlation between Stabilized Sub-pixel precision IPM Images. In: IEEE Proc. Int. Conf. on Robotics and Automation, pp. 2223–2228 (2005)
31. Muad, A.M., Hussain, A., Samad, S.A., Mustaffa, M.M., Majlis, B.Y.: Implementation of Inverse Perspective Mapping Algorithm for the Development of an Automatic Lane Tracking System. In: IEEE Proc. Region 10 Conference (TENCON), vol. 1, pp. 207–211 (2004)

Author Biographies

Marcos Nieto received the Ingeniero de Telecomunicación degree in 2005 from the E.T.S. Ing. Telecomunicación (ETSIT) of the Universidad Politécnica de Madrid (UPM), Spain. He started his Ph.D. studies in 2005 within the Grupo de Tratamiento de Imágenes (GTI, Image Processing Group) in the ETSIT-UPM to obtain the Doctor Ingeniero de Telecomunicación at the Department of Signals, Systems, and Communications of the ETSIT-UPM. In 2010, he joined Vicomtech-ik4 research center, in which he is working in the area of Intelligent Transportation Systems and Engineering. His actual research interests include the use of optimization methods for probabilistic models in computer vision as well as the design of H.264/AVC video codecs.

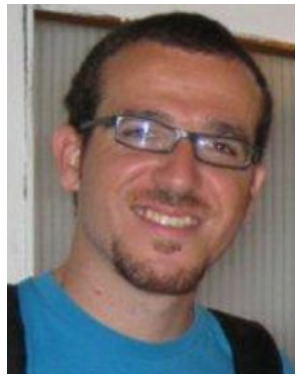

Jon Arróspide Laborda received the Ingeniero de Telecomunicación degree in 2006 from the TECNUN School of the Universidad de Navarra, in San Sebastian, Spain. He worked at the Fraunhofer Institut für Integrierte Schaltungen in Erlangen (Germany), and enrolled in the company Indra Sistemas S.A. during 2006–2007. Since 2007, he is a member of the Grupo de Tratamiento de Imágenes (GTI, Image Processing Group) of the Universidad Politécnica de Madrid (UPM), where he is currently working as a Ph.D. student. He also obtained a M.Sc. in Communication Technologies and Systems from the UPM in 2009. His research focuses on object detection and tracking, especially related to intelligent transport systems.

Luis Salgado received the Ingeniero de Telecomunicación degree in 1990 and the Ph.D. degree in communications with (summa cum laude) in 1998, both from the E.T.S. Ingenieros de Telecomunicación, Universidad Politécnica de Madrid (UPM), Spain. Since 1990, he has been a member of the Grupo de Tratamiento de Imágenes (GTI, Image Processing Group) of the UPM. He was a Ph.D. scholar of the Spanish National Research Plan from 1991 to 1994, and a research assistant from 1995 to 1996. Since 1996, he has been a member of the faculty of the UPM, formerly as a teaching assistant, and currently as an associate professor (tenure in 2001) of Signal Theory and Communications in the Department of Signals, Systems, and Communications. He is associate editor of the Journal of Real-Time Image Processing, has been member of the Scientific and Program Committees of several international conferences and has been auditor and evaluator of European research programs since 2002. He has participated in many national and international research projects, and his professional interests include video analysis, processing and coding.